Title

Inferring Pattern and Disorder in Close-Packed Structures from X-ray Diffraction Studies, Part II: Structure and Intrinsic Computation in Zinc Sulphide

Authors

Varn, DP
Canright, GS
Crutchfield, JP

Publication Date

2003-02-27

Peer reviewed

Acta Crystallographica Section B
Structural Science
ISSN 0108-7681
Editor: **Carolyn P. Brock**

Inferring planar disorder in close-packed structures *via* ε-machine spectral reconstruction theory: structure and intrinsic computation in zinc sulfide

D. P. Varn, G. S. Canright and J. P. Crutchfield

Acta Crystallographica Section B
Structural Science
ISSN 0108-7681

Inferring planar disorder in close-packed structures *via* ε-machine spectral reconstruction theory: structure and intrinsic computation in zinc sulfide

D. P. Varn,[a,b,c]* G. S. Canright[c,d]* and J. P. Crutchfield[b,e]*

[a]Max-Planck-Institut für Physik komplexer Systeme, Nöthnitzer Strasse 38, 01187 Dresden, Germany, [b]Santa Fe Institute, 1399 Hyde Park Road, Santa Fe, NM 87501, USA, [c]Department of Physics and Astronomy, University of Tennessee, 1408 Circle Drive, Knoxville, TN 37996, USA, [d]Telenor Research and Development, 1331 Fornebu, Oslo, Norway, and [e]Computational Science and Engineering Center and Physics Department, University of California, One Shields Avenue, Davis, CA 95616, USA

Correspondence e-mail: dpvarn@pks.mpg.de, geoffrey.canright@telenor.com, chaos@cse.ucdavis.edu

Received 9 March 2006
Accepted 17 October 2006

We apply ε-machine spectral reconstruction theory to analyze structure and disorder in four previously published zinc sulfide diffraction spectra and contrast the results with the most common alternative theory, the *fault model*. In each case we find that the reconstructed ε-machine provides a more comprehensive and detailed understanding of the stacking structure, often detecting stacking structures not previously found. Using the ε-machines reconstructed for each spectrum, we calculate a number of physical parameters – such as configurational energies, configurational entropies and hexagonality – and several quantities – including statistical complexity and excess entropy – that describe the intrinsic computational properties of the stacking structures.

1. Introduction

In several companion papers (Varn *et al.*, 2002, 2007*a*,*b*) we presented a novel technique for the discovery and description of planar disorder in close-packed structures (CPSs): ε-machine spectral reconstruction theory (εMSR or 'emissary'). We showed that the technique allows a unique, minimal and optimal model (an ε-machine) to be built up of a material's stacking structure from diffraction spectra. In this sequel we demonstrate the technique using diffraction spectra from single crystals of disordered, polytypic zinc sulfide (ZnS). Since the discovery of *polytypism* in mineral ZnS crystals (Frondel & Palache, 1948, 1950), much theoretical and experimental effort has been expended to understand this phenomenon (Steinberger, 1983; Mardix, 1986; Sebastian & Krishna, 1994).

ZnS is an attractive system to study for a number of reasons:

(i) *Simplicity of the unit cell and stacking rules*. While many materials are known to be polytypic (Trigunayat, 1991; Sebastian & Krishna, 1994), the constituent *modular layers* (MLs; Varn & Canright, 2001) can have a complicated structure and complex stacking rules (Brindley, 1980; Thompson, 1981; Varn & Canright, 2001). For instance, in ideal micas there are more than a dozen atoms in a unit cell and there are six ways in which two MLs can be stacked. Kaolins and cronstedtites present even more complexity (Varn & Canright, 2001). In contrast, ZnS is simple in the extreme: it is composed of but two atoms – a zinc and a sulfur (Sebastian & Krishna, 1994). They are arranged in a double close-packed hexagonal net, with one species displaced relative to the other by a quarter body diagonal (as measured by the conventional unit cubic cell) along the stacking direction (Shaw & Heine, 1990). We take this double close-packed layer to be an ML (Varn & Canright, 2001). The stacking of MLs proceeds as for all CPSs; namely, there are three absolute orientations each ML can

occupy – *A*, *B* and *C* – with the familiar stacking constraint that no two adjacent MLs have the same orientation.

(ii) *Complex polytypism*. ZnS is one of the most polytypic substances known with over 185 identified crystalline structures (Mardix, 1986; Trigunayat, 1991; Sebastian & Krishna, 1994). Of these, only about a dozen fairly short-period polytypes (up to 21 MLs) are common in mineral ZnS, with the remainder found in synthetic crystals. Some of the crystal structures have repeat distances that extend over 100 MLs. Also, many structures show considerable planar disorder. The wide diversity of structural complexity remains one of the central mysteries of polytypism.

(iii) *Solid-state transformations*. It is believed that there are only two stable phases of ZnS: the low-temperature modification – the β-ZnS or *sphalerite* (3C[1]) – and the high-temperature modification – *wurtzite* (2H) or α-ZnS (Sebastian & Krishna, 1994). The former transforms enantiotropically into the latter at 1297 K. The plethora of structures suggests that most of them are not in equilibrium, but are rather structures that are trapped in a local minimum of the free energy and lack the necessary activation energy to explore all of the configuration space. It is possible to observe these structures by annealing and then arresting the transformation by quenching. One can then study the various intermediate stages of the transformation.

(iv) *Availability*. Polytypes of ZnS, both ordered and disordered, are easily manufactured in the laboratory by a variety of methods (Sebastian & Krishna, 1994). One of the more common methods is growth from the vapor phase above temperatures of $\sim$1373 K. Crystals can also be grown from the melt at high pressures by the use of chemical transport, and hydrothermally. The distribution of the polytypes observed depends on the method used.

Nearly a dozen theories have been proposed to explain polytypism, among them being the ANNNI model (Price & Yeomens, 1984; Yeomans, 1988), Jagodzinski's disorder theory (Jagodzinski, 1954) and Frank's screw dislocation theory (Frank, 1951). For a complete discussion, see for example, Verma & Krisha (1966), Trigunayat (1991) and Sebastian & Krishna (1994). We will comment very little on the mechanisms that *produce* various polytype structures. Instead, our focus will be on describing the disordered structures so commonly seen. We feel that an adequate description of the disordered structures – which so far has been lacking – is warranted before the models that seek to explain the mechanisms that drive the formation of disordered structures can be evaluated, and, especially, the solid-state phase transitions which lead to them.

Previous descriptions of planar disorder in single crystals of ZnS fall into one of two categories: the *fault model* (FM; Varn *et al.*, 2002, 2007*a*) and Jagodzinski's *disorder model* (DM; Jagodzinski, 1949*a*,*b*,*c*; Frey *et al.*, 1986). Applications of the FM include Roth's study of faulting induced in hexagonal crystals grown from the vapor phase upon annealing (Roth, 1960). Roth extracted correlation information from the diffraction spectra by Fourier analysis and then derived analytical expressions relating how correlation functions decayed with both increasing separation between MLs and as a function of the fault probability. He considered both randomly distributed growth and deformation faults and found that for weakly disordered specimens deformation faulting gave the best agreement with experiment.

Significant applications of the FM to planar disorder in ZnS have been carried out by Sebastian, Krishna and coworkers. They studied the 2H-to-3C solid-state transformation in vapor-grown ZnS crystals after annealing between temperatures of 673 and 923 K (Sebastian *et al.*, 1982). By analyzing and comparing the profiles of the integer-*l* reflections[2] with those of the half-integer-*l* reflections for weakly faulted crystals, they found that the disorder was largely due to the random insertion of deformation faults. They attributed slight discrepancies between the observed and calculated profiles to the so-called nonrandom insertion of faults. Sebastian and Krishna later studied the disordered stacking in 3C crystals grown from the vapor phase, as well as those obtained from annealing 2H crystals (Sebastian & Krishna, 1984). They found that the structures of both the as-grown and annealed crystals were best explained as randomly distributed twin faults in the 3C structure. They concluded that the 2H-to-3C transformation in ZnS was proceeded by the nonrandom nucleation of deformation faults occurring preferentially at two ML separations.

To better understand the nature of the nonrandom insertion of deformation faults in the 2H structure, Sebastian and Krishna introduced a three-parameter model that assigned separate probabilities to the random insertion of deformation faults, as well as deformation faulting at two and three ML separations (Sebastian & Krishna, 1987*a*,*b*). They derived analytical expressions for the diffraction spectra in terms of these parameters and concluded that both the 2H-to-3C and the 2H-to-6H transformations proceeded *via* the nonrandom nucleation of deformation faults. Their analysis showed that these transformations occurred simultaneously in different regions of the same crystal. They attributed this to variations in the stoichiometry. Sebastian (1988) gave a similar treatment that came to the same conclusions. With the exception of Roth, all of these analyses depended on carefully characterizing the change in Bragg peaks as a small amount of disorder was introduced. We have previously criticized the FM approach elsewhere (Varn *et al.*, 2002, 2007*a*).

Jagodzinski's DM is a two-parameter model that assumes two thermodynamically stable phases in CPSs: 2H and 3C. Therefore, two kinds of fault are found (*i.e.* structure and not mechanism): namely, cubic faults in 2H and hexagonal faults in 3C. By choosing appropriate values for the two model parameters model 4H structures can also be modeled. Within this framework, an analytical expression for the diffracted inten-

[1] We use the Ramsdell notation to specify common crystal structures in CPSs (Varn *et al.*, 2007*a*).

[2] The notation and definitions of the variables used here have been introduced elsewhere (Varn *et al.*, 2007*a*). Also note that our definition of *l* differs slightly from that used by other authors.

sity is derived that depends on the model parameters in a complicated manner. Nonetheless, model parameters can be selected that give the best agreement with experiment.

Müller (1952) used this method to analyze faulted ZnS diffraction spectra and found that while he was able to obtain reasonable agreement between theory and experiment for a few spectra, for many he was not. Singer & Gashurov (1963) re-examined this approach and concluded that the DM applies when faulting is random, but when the faulting is nonrandom, as it is suspected to be in many ZnS specimens, the model fails. However, Frey *et al.* (1986) studied the 3C-to-2H transformation in single crystals of ZnS using the DM and were able to obtain excellent agreement between theory and experiment. They fit the experimental diffraction spectrum to the analytical one of the DM. Owing to the complicated nature of the expression, however, they treated eight constants that depend on the two model parameters as independent. From these eight fitted parameters they were able to find the two model parameters that best fit each spectrum.

However, questions must be raised concerning the mathematical rigor used to find the model parameters in this way. The description of the stacking disorder as given by the DM is a special constrained case of the $r = 2$ computational mechanics approach. As in the latter, in the DM there is no assumption of weak faulting and diffuse scattering is used to build the model. Since the spectra we analyze have not been previously treated using the DM and it is a special case of our own, the DM is not discussed further here.

A third possible method of discovering structural information on disordered solids from diffraction spectra employs a reverse Monte Carlo (RMC) technique (Keen & McGreevy, 1990; Proffen & Welberry, 1998; Welberry & Proffen, 1998). In this method one typically searches for a configuration of constituent atoms such that a signal, *e.g.* the diffraction spectrum, estimated from the candidate structure most closely matches the experimental signal. Notably, this technique can be applied to disorder in three dimensions. One drawback, however, is that candidate structures are often found that are physically implausible. One needs to impose assumptions to eliminate these. The application of RMC to layered solids is a subject of current research (Varn & Crutchfield, 2006).

In this work, we apply computational mechanics (Crutchfield & Young, 1989; Feldman & Crutchfield, 1998; Shalizi & Crutchfield, 2001) to discover and describe disordered stacking sequences in four previously published ZnS diffraction spectra. A Fourier analysis was carried out on each spectrum to find correlation information between MLs and then the probability distribution of the stacking sequences was calculated. From the latter we reconstruct the ε-machine that gives the stochastic process for the ML stacking and compare it to previous FM analyses. From the reconstructed ε-machine, the configurational entropy per layer, average configurational energy per Zn–S pair, memory length, hexagonality and generalized period (Varn *et al.*, 2007*b*) were calculated for the first time. The diffraction spectra of the four samples are well described using the computational mechanics approach.

We note that our primary purpose in the following is expository; that is, we wish to demonstrate the efficacy of εMSR on actual materials. Since we use diffraction spectra from older studies (Sebastian & Krishna, 1994), the analyses given here are less than ideal. Specifically, we digitized data from published spectra and found that there was significant systematic error in each original spectrum. Additionally, the experimental data were not reported with error bars. Despite these possible shortcomings, εMSR allows us to offer more comprehensive structural and physical analyses of the spectra than given by previous workers.

Our development is organized as follows. In §2 we outline our approach, including a brief discussion of the experimental methods, and our analysis. In §3 the results of ε-machine reconstruction for four experimental ZnS diffraction spectra are given, compared with the FM approach wherever possible. In §4 we calculate the configurational energies per Zn–S pair and the hexagonality for the various structures from our reconstructed ε-machines. In §5 we give our conclusions and propose some directions for future theoretical and experimental work.

2. Methods

The four diffraction spectra we analyze originate from Sebastian & Krishna (1994) and are labeled SK*XXX* by the page (*XXX*) on which they appear in that source. These data were collected in the 1980s and since they no longer exist in numerical form (Sebastian, 2001), we digitized them from the diffractograms given in the Sebastian and Krishna publication (Sebastian & Krishna, 1994). For each diffraction spectrum, the digitization process typically resulted in 200–500 data points. We further performed a linear interpolation between these points so that our representation of each experimental diffraction spectrum consisted of data points separated by $\Delta l \simeq 0.0001$. In all the numerical analyses we used this finer mesh. However, for the sake of clarity, when we visually compare the diffraction spectra generated from εMSR with experimental spectra, we only display representative experimental points.

In this section we give a brief synopsis of the experimental procedure, discuss the assumptions made to analyze the data and list the corrections applied to the experimental spectra.

2.1. Experimental details

The experimental procedure is given in more detail elsewhere (Sebastian & Krishna, 1994, 1987*b*; Sebastian *et al.*, 1982; Sebastian, 1988). Briefly, the crystals were grown from the vapor phase at a temperature in excess of 1373 K in the presence of H_2S gas. Each crystal was needle-shaped, approximately 0.1–0.4 mm in diameter and 1–2 mm in length. Two of the four crystals were further annealed for 1 h at 573 and 773 K. These investigations were performed to better understand the fault structures they contain, as well as study the solid-state transformations that ZnS crystals undergo.

The intensity along the 10.l reciprocal lattice row was recorded using a four-circle single-crystal diffractometer for each specimen in steps of approximately $\Delta l = 0.005$. [Our definition of l differs slightly from that of Sebastian & Krishna (1994) so the l-increment we report also differs.] The crystal and the counter were held stationary while the crystal was illuminated with Mo $K\alpha$ radiation. The sharp reflections along the $h - k = 0$ (mod) 3 rows were used to orientate each crystal. The divergence of the incident beam was adjusted to cover the mosaic spread for each crystal. The experimental diffraction spectrum is reported as the total number of counts *versus* l. The crystals were examined under a vickers projection microscope and did not show signs of kinking or shearing, even after annealing. They did show parallel striations or stripes perpendicular to the stacking direction.

2.2. Assumptions

To make the analysis tractable, we employ the following assumptions which are common in the analysis of planar disorder in ZnS:

(i) *Each ML is perfect and free of distortions and defects*. We assume that each ML is identical and the MLs themselves are free from defects. That is, each ML is crystalline in the strict sense, with no point defects, impurities or distortions in the two-dimensional lattice structure. This clearly precludes the possibility of screw dislocations, which are known to play a role in the polytypism of some ZnS crystals (Sebastian & Krishna, 1994; Michalski, 1988). Since each of the crystals we analyze was examined under a Vickers projection microscope and no such dislocations were seen, and the crystals retained their shape after annealing, this seems reasonable. [It is known (Sebastian & Krishna, 1994) that during the solid-state transformations of specimens of ZnS with an axial screw dislocation, the specimen will exhibit 'kinking' with a characteristic angle of 19° 28′.]

(ii) *The spacing between MLs is independent of the local stacking arrangement*. There is known to be some slight dependence of the inter-ML spacing depending on the polytype (Sebastian, 1988; Sebastian & Krishna, 1994). For the 2H structure in ZnS, the inter-ML spacing is measured to be 3.117 Å. For the 3C structure the cubic cell dimension is $a_c = 5.412$ Å, which gives a corresponding inter-ML spacing of 3.125 Å. Therefore, to an excellent approximation, this spacing is independent of the local stacking environment in ZnS.

(iii) *The scattering power of each ML is the same*. We assume that each ML diffracts X-rays with the same intensity. There is no reason to believe that this is not so, unless absorption effects are important or the geometry of the crystal is such that each ML does not have the same cross-sectional area.

(iv) *The stacking faults extend over the entire fault plane*. Examination under microscope indicates that this is generally true. However, Akizuki (1981) found evidence that the faults do not extend completely over the faulted MLs by examining a partially transformed ZnS crystal under an electron microscope.

(v) *The 'stacking process' is stationary*. We simply mean that the faults are uniformly distributed throughout the crystal. In other words, we assume that the probability of finding a particular stacking sequence is independent of its location in the crystal. This does not, however, preclude regions of crystalline structure interspersed between regions of disorder. It simply means that the statistics of the stacking do not change from one end of the crystal to the other.

Notably absent from this list are any assumptions on the crystal structure present (if any) and how the sample might deviate from that structure. In contrast to the FM, we invoke no *a priori* structural assumptions concerning the stacking sequence.

2.3. Corrections to the experimental spectra

We corrected each spectrum for the following effects:

(i) *The atomic scattering factor*. This correction accounts for the spatial distribution of electrons, as well as for the wavelength of the incident radiation and angle of reflection. Calculations of these effects are given in standard tables (Hahn *et al.*, 1992) and we employ them in our work.

(ii) *The structure factor*. The structure factor (Sebastian & Krishna, 1994) accounts for the two-atom basis in ZnS.

(iii) *Anomalous scattering factors*. Also called dispersion factors, the anomalous scattering factors correct for the binding energy of the electrons and the phase shifts (Hahn *et al.*, 1992). For our case, we find these to be small, but have included them nonetheless.

(iv) *Polarization factor*. We use the standard correction factor for unpolarized radiation (Warren, 1969).

Factors we did not correct for include the following:

(i) *Thermal factors*. At room temperature, this effect is small for ZnS (Varn, 2001).

(ii) *Absorption factor*. For the geometry of the ZnS crystals we analyzed, the linear mass coefficient (Woolfson, 1997; Milburn, 1973) is much larger than the thickness, therefore, we ignore it.

(iii) *Instrument resolution*. This is not reported with the experimental data, so we do not deconvolve the spectrum.

3. Analysis

The structural analysis of four experimental diffraction spectra taken from Sebastian & Krishna, (1994) is now discussed. εMSR was applied to each spectrum to build a model that describes the stacking process (Varn *et al.*, 2007*a*). From our model, various measures of intrinsic computation were calculated for each spectrum. The results were compared with those obtained by previous researchers using the FM. Since the experimental spectra were not reported with error bars, we were unable to set an error threshold Γ, as required in εMSR. Instead, we found that each increase in memory length r continued to give a better description of each spectrum (Varn, 2001). We performed εMSR up to $r = 3$ for each spectrum. Note that at $r = 3$, the resulting ε-machine is

specified by $2^3 = 8$ parameters. To find the correlation functions (CFs) from the ε-machines, we used a sample length of 400 000 MLs, as generated by the ε-machine. The diffraction spectra were calculated using 10 000 MLs. The experimental spectra were normalized to unity over the l interval used for reconstruction, as were the spectra calculated from each ε-machine. For the spectra calculated from the FM, we set the overall scale to best describe the Bragg peaks, as shown in Sebastian & Krishna (1994). We also calculated the profile $\mathcal{R}$ factor (Varn *et al.*, 2007*a*) to evaluate the agreement between experiment and theory for each spectrum.

Note that we have previously discussed two of the spectra, SK134 and SK135 (Varn *et al.*, 2002). Here we present the background for claims made in the previous paper, as well as provide a more in-depth analysis.

3.1. SK134

The corrected diffraction spectrum along the 10.l row for an as-grown 2H ZnS crystal is shown in Fig. 1. One immediately notices that the spectrum is not periodic in l, as it should be, but instead suffers from variations in the intensity. The peaks at $l = 0.0$ and $l = 1.0$ are of similar intensity, but the peaks at $l = -0.5$, 0.5 and 1.5 seem to suffer from a steady decline in intensity. We can therefore be confident that this spectrum contains substantial systematic error, as reported by the experimentalists.

This difference in diffracted intensity between peaks results from the finite thickness of the Ewald sphere owing to the divergence of the incident beam (Sebastian & Krishna, 1987*b*, 1994). A suitable choice of geometry can minimize, but not eliminate, these effects such that only a gradual variation in I with Δl is found. Since analysis by the FM depends only on the change in shape and the position of the Bragg-like peaks, such a slow variation of the diffracted intensity with l will not affect the conclusions drawn from an FM analysis. It is possible to correct these effects (Pandey *et al.*, 1987; Sebastian & Krishna, 1994), but this has not been carried out according to the literature.

Our analysis depends on selecting an appropriate l interval where variations in diffracted intensity owing to these experimental effects are minimized. It is important then to select an interval that is relatively error-free. There are two criteria, termed *figures-of-merit* and denoted γ and β, that can be used for this (Varn *et al.*, 2007*a*). It can be shown that in an error-free spectrum the parameters must be equal to the constant values $-\frac{1}{2}$ and 1, respectively, for *any* unit l interval, regardless of the amount of planar disorder present. The extent that β and γ differ from their theoretical values over a given l interval measures how well the diffraction spectrum over the interval can be represented by a physical stacking of MLs. It makes sense then to choose an l interval for ε-machine reconstruction such that the theoretical values of the figures-of-merit are most closely realised. This does not, of course, guarantee that the interval is error-free. Glancing at Fig. 2 shows that $\gamma = -0.51$ and $\beta = 0.95$ over the interval $l \in [0.04, 1.04]$.

We perform εMSR (Varn *et al.*, 2007*a*) and find that the smallest-r ε-machine that gives reasonable agreement between the measured and ε-machine spectra has a memory length of $r = 3$. The reconstructed ε-machine is shown in Fig. 2 of Varn *et al.* (2002). The large asymptotic state probabilities for the C and H causal states (CSs), as well as the large inter-state transition probabilities between them, indicate this is predominantly a 2H crystal. More specifically, the probability of sequences 1010 and 0101 appearing, corresponding to the 2H crystal structure, have a combined total weight of about 64%. The remaining probability is distributed among the other 14 length-4 sequences. It is tempting to interpret the remaining structure in terms of faults and, indeed, it seems we can.

Let us treat the transitions $s = 0$ from causal state E and $s = 1$ from state F as though they are missing for the purposes of a fault analysis. This implies that the sequences 0001 and 1000 are disallowed. Of course, this cannot be exactly true, as the CS F would then be isolated from the rest of the ε-machine. In this case, the ε-machine would not be strongly

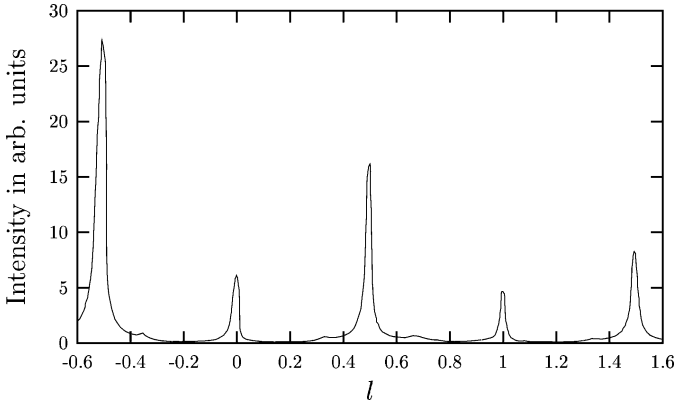

Figure 1
Diffraction spectrum along the 10.l row from SK134 corrected for atomic scattering factors, the structure factor, dispersion factors and the polarization factor (Hahn *et al.*, 1992; Woolfson, 1997; Warren, 1969). We see that the spectrum is not periodic in l, as it should be. This indicates that significant errors exist in the data.

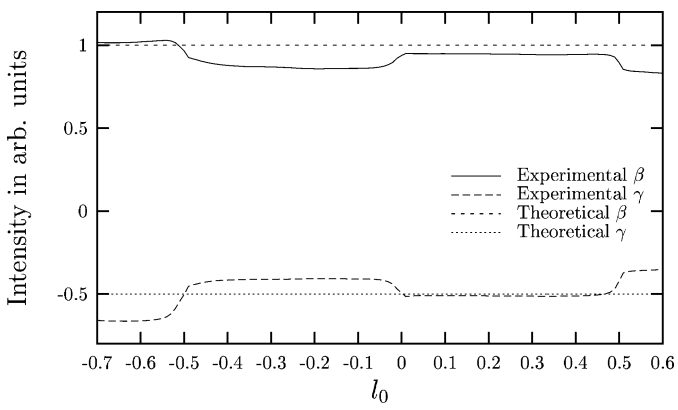

Figure 2
Experimental and theoretical figures-of-merit – β and γ – as a function of l_0 for the diffraction spectrum SK134. We define l_0 as the point at which integration over a unit l interval is initiated. We find that $l_0 \approx 0.04$ gives the best agreement with the theoretical values.

Table 1
Structural decomposition of SK134 according to the reconstructed ε-machine of Fig. 2 of Varn *et al.* (2002) and according to the fault model analysis of Sebastian & Krishna (1994).

The latter is valid only under the assumption of weak faulting (reproduced from Varn *et al.*, 2002).

Structure	ε-Machine (%)	Fault model (%)
2H	64	83
3C	8	0
Deformation fault	16	17
Growth fault	6	0
Layer-displacement fault	6	0

connected and, as such, cannot represent a physical stacking of MLs. However, the combined probability weight of these two sequences is < 1%, so neglecting them gives only a small error in our intuitive understanding of the faulting structure.

On the left half of the ε-machine, there is a structure associated with a 2H deformation fault [ABCD] with probability weight 0.16 = $P(1011) + P(0111) + P(1110) + P(1101)$. We can interpret the causal-state cycle (CSC) [DBEGHC] as a layer-displacement fault and see that it is assigned a probability weight of 0.06. The right portion contains the CSC [EGH] with probability weight 0.06, which is associated with growth faults. The CSCs [A] and [F], identified as the 3C structure, have a combined weight of 0.08.

Given these observations, a possible interpretation suggested by the ε-machine is that SK134 has crystal structures and faults in the proportions given in Table 1. The decomposition present is reasonable since there is an underlying crystal structure present and the smaller, faulting paths are not very probable. As we will see, this need not always be the case. Sebastian & Krishna (1994) have analyzed this diffraction spectrum using the FM and found that approximately one in every 20 MLs is deformation faulted, so they described the stacking structure as a faulted 2H crystal with 5% random deformation faulting. This is equivalent to assigning CSCs

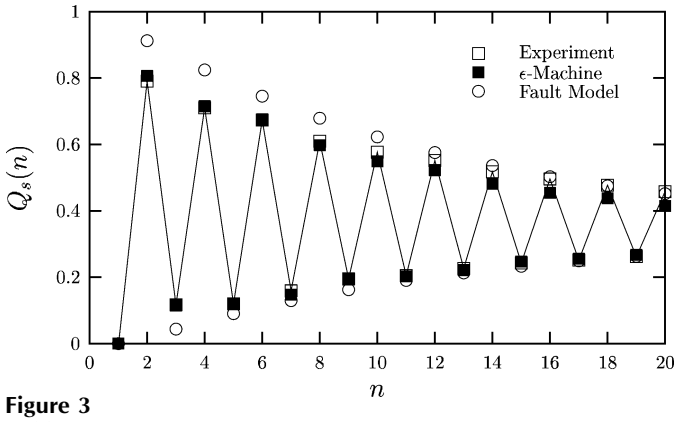

Figure 3
$Q_s(n)$ *versus* n for experimental spectrum SK134 (open squares connected by solid line), the fault model (open circles) and the $r = 3$ ε-machine (solid squares). The $Q_s(n)$ are defined only for integer values of n, but lines are drawn connecting adjacent points as an aid to the eye. We see good agreement up to $n \simeq 15$, after which the $r = 3$ approximate correlation functions decay too quickly to their asymptotic value of 1/3.

responsible for deformation faulting a total probability weight of 0.17.

We compare the structure analyses of the two models in Table 1. We see that both analyses agree that the dominant structure is 2H, although the ε-machine attributes less of the crystal structure to this 'parent' phase. Similarly, both find that structures associated with deformation faulting are important and assign them almost equal weights.

They differ, however, in that the ε-machine finds additional faulting structures (growth and layer-displacement faulting), as well as the 3C crystal structure. Since this crystal will transform into a twinned 3C structure, if annealed at sufficiently high temperatures for long enough, the latter is easily understood as a nascent structure in that process. Discovering the presence of a weak 3C structure is not unreasonable since there is some slight enhancement of the diffracted intensity at $l \simeq 1/3$ and $l \simeq 2/3$. The other faulting structures seen are less easily understood. Growth faults, so-named because they primarily are formed during the growth of the 2H crystal, are not expected to play an important role in the solid-state transformations of ZnS (Roth, 1960). Their presence here may result from the initial growth of the crystal. The small amount of layer-displacement structure could be seen as two adjacent, yet oppositely oriented, deformation faults. That is, a deformation fault in a 2H structure is simply a spin flip in the Hägg notation (Varn *et al.*, 2007*a*), so that the sequence ...010101... transforms to ...011101... as a result of one deformation and then to ...011001... upon another resulting in a layer-displacement fault: ...011001.... This might imply some coordination between faults. Alternatively, the mechanism of layer-displacement faulting may play some minor role in the solid-state transformation.

However, one cannot disambiguate these from the available spectra and the reconstructed ε-machine. The ε-machine only provides information on the structure. We must look outside the ε-machine to formulate an understanding of *how* the polytype came to be stacked in this way. This is the critical difference between faulting *mechanism* and faulting *structure*. In the former, a physical process is responsible for causing the MLs to shift or deviate from a perfect crystal. In the latter, within the limit of weak faulting, the physical process leads to a given (statistical) structure. In this limit it may be possible to postulate with some certainty that the mechanism resulted in the observed structure. For more heavily faulted crystals, however, such an identification of structure with mechanism is dubious. Other techniques, such as numerical simulations (Kabra & Pandey, 1988; Engel, 1990; Shrestha *et al.*, 1996; Shrestha & Pandey, 1996*a*,*b*, 1997; Gosk, 2000, 2001) or analysis of a series of crystals in various stages of the transformation, are necessary to unambiguously determine the mechanism (Varn & Crutchfield, 2004).

Returning to the analysis of SK134, Fig. 3 compares the CFs obtained from the experimental diffraction spectrum, those obtained from the ε-machine and those from the FM. There is reasonable agreement between the experimental and ε-machine-predicted CFs. For small n, however, the FM overestimates the amplitude in the oscillations in $Q_s(n)$.

The experimental diffraction spectrum is compared with that calculated from the FM and from the ε-machine in Fig. 1 of Varn *et al.* (2002). Both models give good agreement near the Bragg peaks at $l = 0.5$ and $l = 1.0$, with perhaps the FM performing a little better at $l = 1.0$. The diffuse scattering near the shoulders of the $l = 0.5$ peak are better represented by the ε-machine. We calculate the profile $\mathcal{R}$ factor between experiment and the FM to be $\mathcal{R}_{\rm FM} = 33\%$ and between experiment and εMSR to be $\mathcal{R}_{\epsilon M} = 20\%$.

So, our analysis of SK134 is an improvement over the FM analysis in several important ways.

(i) Even in the limit of weak faulting, εMSR finds closer agreement with experiment than the FM, as measured by the profile $\mathcal{R}$ factors.

(ii) Again in the limit of weak faulting, the ε-machine can be decomposed (although not necessarily uniquely) to give an estimate of the crystal and fault structure present.

(iii) As such, we were able to identify and quantify several additional structures in the crystal, namely the presence of a small amount of 3C crystal, growth and layer-displacement faults.

3.2. SK135

The next sample we examine is a twinned 3C crystal obtained by annealing a 2H crystal at 773 K for 1 h. The diffraction spectrum for this crystal is given in Fig. 3 of Varn *et al.* (2002). We find that the figures-of-merit are closest to their theoretical values over the interval $l \in [-0.80, 0.20]$ with values $\beta = -0.50$ and $\gamma = 0.93$. The smallest r ε-machine that gives reasonable agreement with experiment was found at $r = 3$ and has a profile $\mathcal{R}$ factor of $\mathcal{R}_{\epsilon\rm M} = 13\%$. The resulting ε-machine is shown in Fig. 4 of Varn *et al.* (2002). Based on the presence of asymmetrically broadened peaks and the absence of peak shifts, an FM analysis (Sebastian & Krishna, 1994) finds this sample to be a twinned 3C crystal with 12% twinned faulting. The profile $\mathcal{R}$ factor between experiment and the FM is found to be $\mathcal{R}_{\rm FM} = 33\%$.

The large CS probabilities associated with CSs A and F, as well as their large self-loop transition probabilities, suggest that this is a twinned 3C crystal. We also note that the transitions corresponding to antiferromagnetic paths (0101 and 1010) have a relatively small combined weight of only about 4%. In fact, the probability weight for the 0101 path is zero. (The transition from CS H to CS C is missing.) This indicates that the 2H structure has largely been eliminated. In addition to the 0101 path, the 1001 and 0010 paths are also missing. This implies that twinned faulting is important, but also the remnant of the 1010 path has some role. Instead of a simple twinned fault [ABEF] giving the sequence $\ldots 1111|00000\ldots$, where the vertical line indicates the fault plane, the path [ABCHEF] giving the sequence $\ldots 1111|01000\ldots$ has approximately twice as much probability weight associated with it. In the ε-machine's right portion twinned faulting [FGDA] is largely responsible for the (0)* 3C cycle converting to the (1)* 3C cycle, and we also observe that double deformation faulting [FGDBE] plays a role.

It is interesting to mention that while an ML of ZnS has spin-inversion symmetry (Varn & Canright, 2001) and, thus, the one-dimensional Hamiltonian describing the energetics of the stacking is also spin-invariant, in general ε-machines need not be spin-inversion invariant. (Note that the ε-machine in Fig. 4 of Varn *et al.*, 2002, is *not* spin-inversion invariant.) There is, of course, no reason why one should demand spin-inversion invariance. After all, then one could never have a crystal of purely one 3C structure or the other. However, since this crystal was initially in the 2H structure – which is spin-inversion invariant – it is curious that this is not preserved as the crystal is annealed. That is, there is no reason to expect that faulting should occur preferentially with one chirality. Notably, the FM *always* assumes spin-inversion symmetry.

Examining the CF $Q_s(n)$ estimated from experiment with those found from the ε-machine in Fig. 4, we find reasonable agreement up to $n \simeq 20$. The $Q_s(n)$ found from the FM generally overstate the magnitude of the oscillations in the CFs.

We can further examine the diffraction spectra. In Fig. 3 of Varn *et al.* (2002), the diffraction spectrum found from the FM and the ε-machine are compared with experiment. The ε-machine gives a good fit, except perhaps at a shoulder in the experimental spectrum at $l = -0.6$ and the small rise at $l = -0.16$. The latter might be understood as a minor competition between the 3C and 6H CSCs that is not being well modeled at $r = 3$. Comparison of the diffraction spectrum from the FM with that from experiment reveals good agreement with the peak at $l = -0.33$ and poor agreement with the one at $l = -0.67$. This is not surprising as the FM did not use the peak at $l = -0.67$ to find the faulting structure. Likewise, the diffuse scattering between peaks is not at all well represented by the FM. Additionally, the small rise in diffuse scattering at $l = -0.16$ is likewise absent in the FM diffraction spectrum.

A comparison between the FM and εMSR analyses of SK135 illustrates several important points.

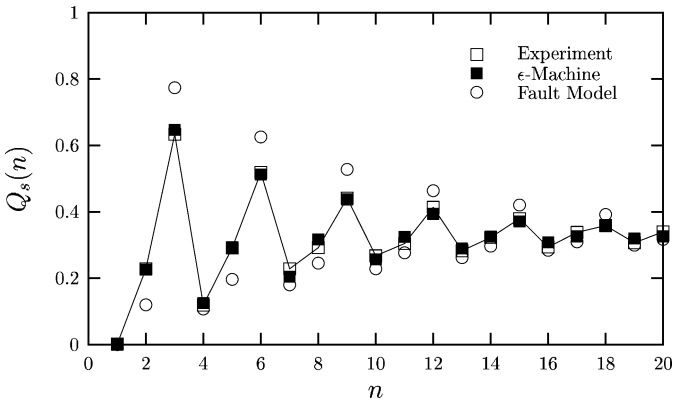

Figure 4
Comparison of the $Q_s(n)$ *versus* n for experimental spectrum SK135 (open squares), the ε-machine (solid squares) and the FM (open circles). The ε-machine gives good agreement with experiment, while the FM overestimates the oscillation magnitude.

(i) This diffraction spectrum shows considerable disorder, and as such the FM is considerably less successful in reproducing the experimental diffraction pattern. ($\mathcal{R}_{\epsilon M} = 13\%$ *versus* $\mathcal{R}_{\rm FM} = 33\%$). Since εMSR does not assume any kind or amount of crystal or fault structure and uses the all the information in the diffraction spectrum, it functions considerably better than the FM for highly disordered crystals.

(ii) Therefore, εMSR captures the diffuse scattering between the Bragg-like peaks much more effectively.

(iii) εMSR shows that the faulting structure between the two 3C crystal structures is not simply due to twin faulting. Rather, the sequence . . . 1111|01000 . . . is more likely than the simpler fault . . . 1111|0000 . . ..

(iv) εMSR does not require spin-inversion symmetry as the FM does.

3.3. SK137

The third experimental spectrum we analyze comes from an as-grown disordered, twinned 3C crystal. The diffraction spectrum for this crystal along the 10.l row is shown in Fig. 5. The figures-of-merit are closest to their theoretical values over the interval $l \in [-0.8, 0.2]$ with values of $\gamma = -0.49$ and $\beta = 0.98$. We performed ε-machine reconstruction up to $r = 3$ and found that this produces reasonable agreement with experiment, giving a profile $\mathcal{R}$ factor of $\mathcal{R}_{\epsilon\rm M} = 17\%$. The $r = 3$ ε-machine is shown in Fig. 6. An FM analysis finds SK137 to be a twinned 3C crystal with 6.8% twinned faulting (Sebastian & Krishna, 1994). The FM calculated diffraction spectrum has a profile $\mathcal{R}$ factor of $\mathcal{R}_{\epsilon M} = 58\%$ when compared with experiment.

A comparison of the CFs from experiment, the FM and the ε-machine is shown in Fig. 7. For smaller n, the ε-machine gives good agreement with experiment, although the error increases at larger n. As shown elsewhere (Varn, 2001), the experimental CFs maintain small, but persistent oscillations about their asymptotic value of 1/3 up to $n \simeq 40$, while the CFs derived from the ε-machine effectively reach this asymptotic value at $n \simeq 25$. This leads us to speculate that there is some structure in the stacking process that the ε-machine is missing. We expect that reconstruction at $r = 4$ will prove interesting here. This has not yet been completed.

The FM fares markedly worse. It substantially overestimates the strength of the oscillations in the CFs for all n.

A comparison of the diffraction spectra for experiment, the FM and the ε-machine is given in Fig. 5. The ε-machine gives reasonable agreement everywhere except around the Bragg peaks at $l = -0.33$ and $l = -0.67$. Here the ε-machine gives a value for the peak intensity 15 and 35% lower, respectively, than experiment. The FM does much better at the Bragg peaks, as one might expect. However, the diffuse scattering between the peaks and especially the broad-band rise in intensity near $l = -0.5$ are simply missing in the FM diffraction spectrum. The ε-machine fit in this region is substantially better, picking up a number of important spectral features, such as broad band components and broadened peaks.

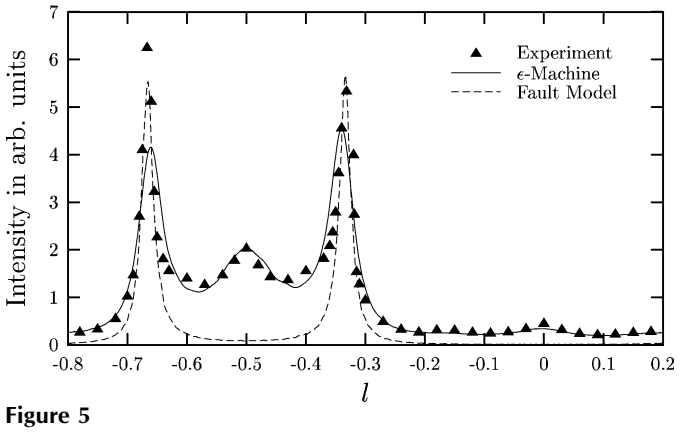

Figure 5
Comparison of the experimental diffraction spectrum SK137 along the 10.l row (triangles) for a disordered 3C single crystal with the diffraction spectra calculated from the FM with 6.8% twinned faulting (dashed line) and the ε-machine (solid line). The profile $\mathcal{R}$ factor between experiment and the ε-machine calculated diffraction pattern is $\mathcal{R}_{\epsilon\rm M}$ = 17%. The FM gives considerably worse agreement, with a calculated profile $\mathcal{R}$ factor of $\mathcal{R}_{\rm FM}$ = 58% between the FM model and experiment.

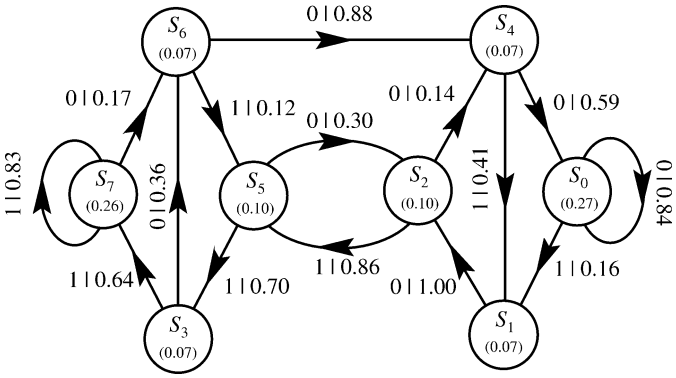

Figure 6
The reconstructed $r = 3$ ε-machine for SK137. The strong self-loop transition probabilities between causal states $\mathcal{S}_0$ and $\mathcal{S}_7$, as well as their large asymptotic state probabilities, suggest that the . . . 0000 . . . and . . . 1111 . . . structures are important. Notice that, unlike the ε-machine for SK135, the CSC $[\mathcal{S}_2\mathcal{S}_5]$ is present, suggesting that the associated 2H structure is present. The absence of the transition between CSs $\mathcal{S}_1$ and $\mathcal{S}_3$ implies that the 0011 sequence, and therefore the CSC associated with the 6H structure, is not present.

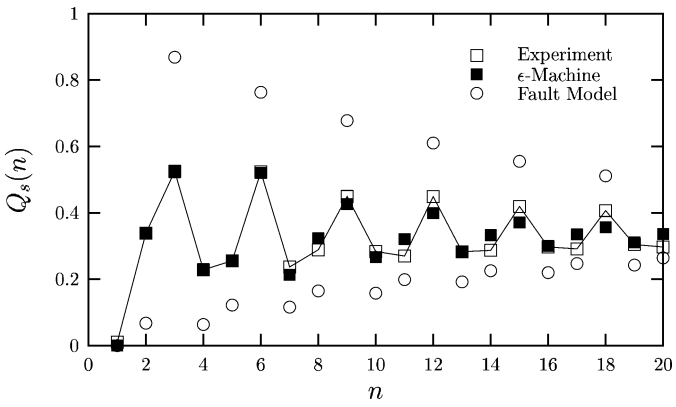

Figure 7
Comparison of the CF $Q_s(n)$ *versus* n experimental spectrum SK137 (open squares), the $r = 3$ approximate ε-machine (solid squares) and the FM (open circles).

Table 2
The FM structural interpretation of the reconstructed ε-machine of Fig. 9.

This is valid only under the assumption of weak faulting.

Structure	Contribution (%)
2H	82
3C	4
Deformation fault	9
Growth fault	4
Other disorder	1

What does the ε-machine imply about the stacking process? All CSs and allowed transitions are present, except for the transition between $\mathcal{S}_1$ and $\mathcal{S}_3$. This absent transition implies that the 0011 stacking sequence is not present in SK137. This then means that the 000111 sequence, and hence the CSC $[\mathcal{S}_7\mathcal{S}_6\mathcal{S}_4\mathcal{S}_0\mathcal{S}_1\mathcal{S}_3]$ associated with the 6H structure (Varn *et al.*, 2006*a*), is also absent. Therefore, in this twinned 3C crystal there is no 6H structure. This is surprising since many ZnS spectra show enhancement about the 6H positions during solid-state phase transitions from 2H to 3C. In Fig. 5 there is (arguably) a slight increase in diffracted intensity at $l = -0.16$ and $l = 0.16$. Therefore, the absence of the 6H structure does seem to be echoed in the experimental spectrum. There is, however, a large broadband increase in intensity about $l = -0.5$ and a much smaller increase about $l = 0.0$. Reflections at these l are usually associated with the 2H structure, with the half-integer peaks carrying three times the intensity of the integer peaks. The ε-machine does show that the CSC $[\mathcal{S}_2\mathcal{S}_5]$ associated with the 2H structure is present. The frequency of occurrence of the 0101 and 1010 stacking sequences together make up about 12% of the total probability weight on the ε-machine. Even though $P_{\rm CSC}([\mathcal{S}_2\mathcal{S}_5]) \ll 1$, it is not unreasonable to suggest that the 2H structure is present.

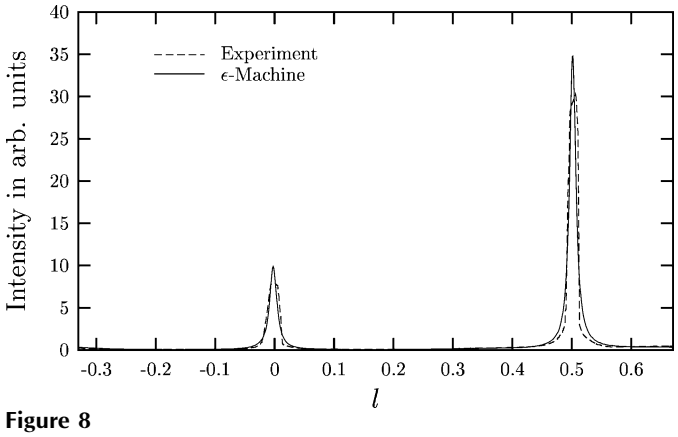

Figure 8
Comparison of the experimental diffraction spectrum SK229 (dashed line) and that calculated from the reconstructed ε-machine (solid line). There is generally good agreement between the two, except that the Bragg-like peaks from the ε-machine are slightly displaced from the experimental spectra and the maximum from the ε-machine overestimates experiment. The ε-machine also has some difficulty reproducing the shape of the experimental spectra. The profile $\mathcal{R}$ factor between the two spectra is $\mathcal{R}_{\epsilon\rm M}$ = 29%.

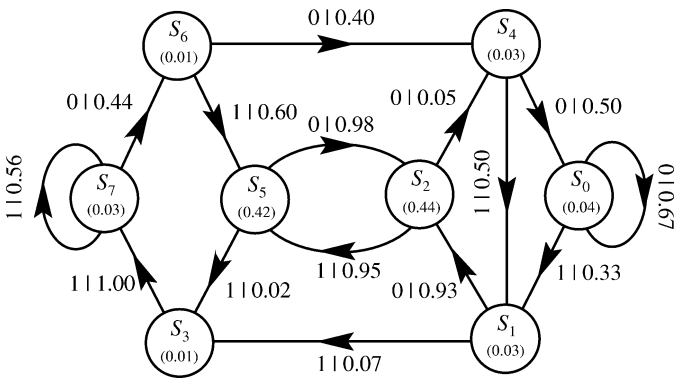

Figure 9
The $r = 3$ ε-machine reconstructed for SK229. The large asymptotic state probabilities for the $\mathcal{S}_2$ and $\mathcal{S}_5$ states, as well as the large state-transition probabilities between them, show that this is predominately a 2H crystal with some faulting.

[Varn *et al.*, 2006*a*], is also absent. Therefore, in this twinned 3C crystal there is no 6H structure. This is surprising since many ZnS spectra show enhancement about the 6H positions during solid-state phase transitions from 2H to 3C. In Fig. 5 there is (arguably) a slight increase in diffracted intensity at $l = -0.16$ and $l = 0.16$. Therefore, the absence of the 6H structure does seem to be echoed in the experimental spectrum. There is, however, a large broadband increase in intensity about $l = -0.5$ and a much smaller increase about $l = 0.0$. Reflections at these l are usually associated with the 2H structure, with the half-integer peaks carrying three times the intensity of the integer peaks. The ε-machine does show that the CSC $[\mathcal{S}_2\mathcal{S}_5]$ associated with the 2H structure is present. The frequency of occurrence of the 0101 and 1010 stacking sequences together make up about 12% of the total probability weight on the ε-machine. Even though $P_{\rm CSC}([\mathcal{S}_2\mathcal{S}_5]) \ll 1$, it is not unreasonable to suggest that the 2H structure is present.

We find several important lessons from the analysis of SK137.

(i) Again, εMSR shows significant improvement over the FM in reproducing the experimental spectrum, especially the diffuse part.

(ii) As with the εMSR analysis of SK134, we find evidence for two crystal structures, both the twinned 3C and the 2H structures.

(iii) εMSR can also exclude the possibility of certain crystal structures, such as the 6H structure, based on the absence of the CSC associated with this crystal structure.

(iv) εMSR can have difficulty in reproducing the Bragg-like peaks, such as those at $l = -0.67$ and $l = -0.33$.

This, coupled with difficulties reproducing the small but persistant oscillation in the CFs at larger n, hints that there are stacking structures that can only be captured at longer memory lengths.

3.4. SK229

Lastly, we examine an as-grown 2H crystal. The diffraction spectrum for this crystal is shown in Fig. 8. We find the figures-of-merit closest to their theoretical values over the interval $l \in [-0.33, 0.67]$ with values of $\gamma = -0.49$ and $\beta = 1.00$. We find that the smallest-r ε-machine that gives reasonable agreement between the measured and ε-machine spectra has a memory length of $r = 3$. The reconstructed ε-machine is shown in Fig. 9. The large asymptotic state probabilities for the $\mathcal{S}_2$ and $\mathcal{S}_5$ CSs, as well as the large inter-state transition probabilities between them, indicate this is predominantly a 2H crystal. More specifically, the probability of seeing sequences 1010 and 0101, corresponding to the 2H cycle, have a combined total weight of $\sim 82.5\%$. The remaining probability is distributed among the other 14 length-4 sequences. It is tempting to interpret the remaining structure as faults and, indeed, we can.

Let us treat the transitions $s = 0$ from $\mathcal{S}_6$ and $s = 1$ from $\mathcal{S}_1$ as though they are missing. These are the least probable

Table 3
A comparison of the three characteristic lengths and three measures of intrinsic computation that one can calculate from knowledge of the ε-machine.

We calculate them for the experimental diffraction spectra, as well as for three crystal structures for reference. Recall that $\Delta = C_\mu - \mathbf{E} - rh_\mu$ (Varn *et al.*, 2007*a*).

System	λ_c	$\mathcal{P}$	r_l	h_μ	C_μ	**E**	Δ
2H	∞	2	1	0	1.0	1.0	0.0
3C	∞	1	0	0	0.0	0.0	0.0
6H	∞	6	3	0	2.6	2.6	0.0
SK134	9.5 ± 0.5	4.8	3	0.50	2.3	0.75	−0.1
SK135	4.4 ± 0.7	5.6	3	0.59	2.5	0.71	0.0
SK137	12 ± 3	6.7	3	0.65	2.7	0.79	0.0
SK229	19 ± 2	3.5	3	0.30	1.8	0.89	0.0

transitions in the ε-machine: $P(0, \mathcal{S}_6) = P(\mathcal{S}_6)P(0|\mathcal{S}_6) \simeq 0.004$ and $P(1, \mathcal{S}_1) = P(\mathcal{S}_1)P(1|\mathcal{S}_1) \simeq 0.002$. Then, in the left half of the ε-machine there is a structure associated with a 2H deformation fault $[\mathcal{S}_7\mathcal{S}_6\mathcal{S}_5\mathcal{S}_3]$ with probability weight $0.040 = P(1011) + P(0111) + P(1110) + P(1101)$. In the right half there is likewise a 2H deformation fault structure $[\mathcal{S}_0\mathcal{S}_1\mathcal{S}_2\mathcal{S}_4]$ with weight $0.049 = \frac{1}{2}P(0100) + P(1000) + P(0001) + \frac{1}{2}P(0010)$. The right portion contains the CSC $[\mathcal{S}_2\mathcal{S}_4\mathcal{S}_1]$ with weight $0.036 = \frac{1}{2}P(0100) + P(1001) + \frac{1}{2}P(0010)$, which is associated with growth faults. The CSCs $[\mathcal{S}_0]$ and $[\mathcal{S}_7]$, identified as the 3C structure, have a combined weight of 0.041. Given these observations, the interpretation suggested by the ε-machine is that SK229 has crystal structures and faults in the proportions given in Table 2. The decomposition there is reasonable since there is an underlying crystal structure present and the smaller faulting paths are not too large.

SK229 has not been analyzed quantitatively using the FM. By comparing the FWHM of the integer-l to half-integer-l peaks, Sebastian & Krishna (1994) concluded that deformation faulting is the primary vehicle responsible for the deviation from crystallinity seen here. We are in agreement, except that we also detect small amounts of the 3C crystal structure and some growth faults.

Fig. 10 compares the CFs from experiment and the ε-machine. The agreement is good, although the reconstructed ε-machine underestimates somewhat the magnitude of the oscillations in $Q_s(n)$. A visual comparison of the experimental diffraction spectrum and that generated from the ε-machine (Fig. 8) shows that there is reasonable agreement. We calculate an $\mathcal{R}$ factor between the two spectra of $\mathcal{R}_{\epsilon M} = 29\%$.

There are some noticeable differences between the two spectra, however. First, we see that Bragg-like peaks in the ε-machine spectrum are slightly shifted from those in the experimental spectrum. Second, the ε-machine spectrum overestimates the maximum intensity in each peak. Third, the peak profiles are qualitatively different. For the ε-machine, the shoulders of the peaks are broader than those of the experiment and the crowns are narrower. Indeed, the peaks in the experimental spectrum appear plateau-like, *i.e.* the sides are very steep and the crown is rounded. It is not known if this results from instrument resolution or if it is a material property.

This example shows that slightly faulted crystals with sharp Bragg-like structures can be difficult to analyze. Certainly, the basic crystal structure is clear, in this case 2H, but a very fine experimental l-mesh is needed to map each Bragg peak. In contrast, highly disordered spectra with significant diffuse scattering are less sensitive to experimental details, such as instrument resolution. For highly diffuse spectra, where the assumptions underlying the FM break down, εMSR both in practice (extraction of correlation information) and in principle (the ε-machine describes any amount of disorder) reaches its full potential.

We, therefore, find two important lessons from the analysis of SK229.

(i) While, in principle εMSR works equally well for both crystalline and highly disordered samples, there are experimental difficulties associated with the former. The Bragg peaks in crystals need to be mapped out very carefully and in clear contrast to any diffuse scattering.

(ii) Again, a sensible decomposition of the ε-machine for a nearly crystalline sample yields a crystal and fault distribution that is likewise sensible.

4. Physics from ε-machines

Now that we have models (ε-machines) for the stochastic processes underlying the observed ML stacking for each sample, we can calculate a range of structural, computational and physical characteristics that describe the stacking patterns and disorder. In Table 3 we list the measures of intrinsic computation and characteristic lengths calculated for each sample, as well as for three crystal structures for comparison.

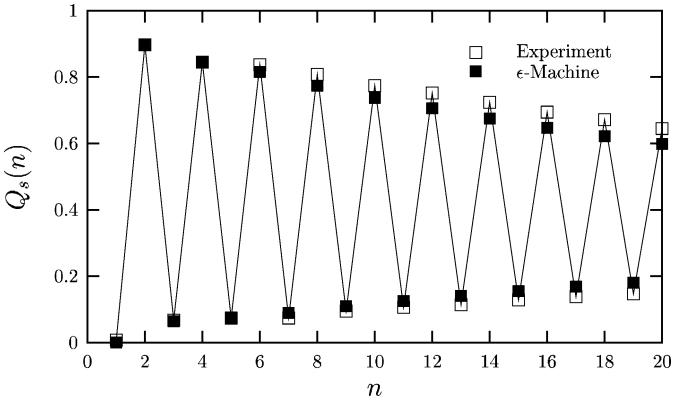

Figure 10
Comparison of the CF $Q_s(n)$ *versus* n experimental spectrum SK229 (solid squares) and the ε-machine (open squares).

Table 4
Relative configurational energies $\tilde{E}$ and hexagonality α_h of experimental polytypes and several pure-crystalline polytypes.

The last column gives the history of each sample, where PC represents perfect crystal, AG as-grown and D disordered. We use the energy coupling constants, J_1 and J_2, calculated by Engels and Needs along with the reconstructed ε-machine for the disordered processes to find the configurational energy of the disordered structures *via* equations (2) and (3)

System	$\langle s_i s_{i+1}\rangle$	$\langle s_i s_{i+2}\rangle$	$\tilde{E}$	α_h	History
2H	−1.00	1.00	1.95	1.00	PC
3C	1.00	1.00	−1.79	0.00	PC
6H	0.33	−0.33	−0.65	0.33	PC
SK134	−0.58	0.63	1.13	0.80	D 2H, 573 K for 1 h
SK135	0.56	0.45	−1.02	0.24	D 2H, 773 K for 1 h
SK137	0.32	0.45	−0.57	0.34	AG 3C
SK229	−0.80	0.86	1.56	0.90	AG 2H

4.1. Characteristic lengths in polytypes

We first note that it was necessary to perform εMSR up to $r = 3$ for each spectrum. This is not surprising since the mechanism of deformation faulting is expected to be important in ZnS, and the minimum ε-machine on which deformation faulting structure can be modeled is $r = 3$. This implies, of course, a longer memory length than either pure 3C or 2H structure alone requires.

The generalized periods (Varn *et al.*, 2007*b*) for the 2H and 3C structures at $\mathcal{P} = 2$ ML and $\mathcal{P} = 1$ ML, respectively, are also much shorter than for the disordered structures which average $\mathcal{P} = 5.7$ ML. This shows that there is spatial organization over a modest range – 6 MLs – for ε-machine-disordered ZnS crystals. This pales in comparison to crystalline polytypes with repeat distances over 100 MLs, but is still much larger than the calculated range of inter-ML interactions of ~ 1 ML (Engel, 1990). We note that many of these long-period crystalline polytypes are believed to be associated with giant screw dislocations that are expressly absent here. For both r and $\mathcal{P}$, the disordered structures have values much closer to that expected for the 6H structure.

In contrast to a perfect crystal, the correlation lengths are finite rather than infinite. Interestingly, the sample that has the most stacking disorder [as measured by h_μ], SK137, also has a comparatively long correlation length. While this was previously classified as an as-grown 3C crystal (Sebastian & Krishna, 1994), we find that it also contains a significant amount of stacking sequence associated with the 2H structure. Since we cannot assume that any of these structures are in equilibrium or the ground state, we can draw no conclusions about the range of inter-ML interactions.

4.2. Intrinsic computation

Each of the diffraction spectra we analyzed also shows considerable stacking disorder. Even a spectrum that is quite crystalline, like SK134, has a configurational entropy of $h_\mu = 0.50$ bits per ML. Of course, for a crystal the entropy rate is zero and for the case of completely disordered stacking one would have $h_\mu = 1$ bits per ML. If we compare SK134 and SK135, each beginning as a 2H crystal but annealed at different temperatures, we see that the latter is slightly more disordered, as we would expect. The statistical complexity, a measure of the average history in MLs needed to predict the next ML, is also relatively constant at 2.3 and 2.5 bits, respectively.

In fact, the measures of intrinsic computation are nearly equal, except those for SK229. However, SK134 and SK135 have very different structures. SK134 is largely 2H in character, while SK135 is largely twinned 3C. Assuming that they were identical before annealing, this would suggest that the disordering process has little effect on these measures. This is, of course, tentative, since such a conclusion can only be drawn after examining many disordered samples. Experimental spectra in the midst of the 2H-to-3C transformation would be of significant interest here. It is possible, though, that SK137 might be such an instance. While this is an as-grown twinned 3C crystal, as noted above, this crystal also has some significant 2H character. Since an earlier analysis (Sebastian & Krishna, 1994) found that both of these were well described by a random distribution of twin faults, they concluded that disordered 3C crystals found in the growth furnace result from a phase transformation from the 2H structure upon cooling the furnace. We find that the two samples (SK135 and SK137), while similar, do have qualitative differences. We can understand this either as a crystal not completely transformed or that the mechanism which created SK137 is not simple. We feel that more experimental data are needed in order to arrive at a more complete understanding. Since $h_\mu = 0.65$ bits per ML for SK137 and is thus more disordered than either SK134 or SK135, the interpretation of this crystal being in the midst of a phase transition is a plausible explanation. The most striking feature of the measures of intrinsic computation is their relative consistency (except for SK229), even while the structure of the crystal changes significantly.

4.3. Configurational energies

One physical quantity amenable to calculation from the ε-machine is the difference in configurational energies of the particular disordered polytypes. Considering possible interactions up to the third nearest neighbor, a first-principles pseudopotential calculation of the total energy of five ZnS polytypes (Engel, 1990) determined that the configurational energy depends only the nearest and the next-nearest neighbors in the stacking arrangement. The most general expression possible for inter-ML interactions up to the third nearest neighbors is given by (Shaw & Heine, 1990)

$$E = E_0 - J_1 \sum_i s_i s_{i+1} - J_2 \sum_i s_i s_{i+2} - J_3 \sum_i s_i s_{i+3} - K \sum_i s_i s_{i+1} s_{i+2} s_{i+3}. \quad (1)$$

Terms with an odd number of spins do not appear owing to symmetry considerations. We take $s_i = \pm 1$ here. It was found that J_1 = 0.00187 eV per Zn–S pair and J_2 = −0.00008 eV per Zn–S pair and that J_3 and K are negligible (Engel, 1990).

Given this let us rewrite (1) in terms of the energy per Zn–S pair and take $E_0 = 0$. The configurational energy is then

$$\tilde{E} = -J_1 \langle s_i s_{i+1} \rangle - J_2 \langle s_i s_{i+2} \rangle, \quad (2)$$

where brackets indicate the expectation value over the stacking sequence. The expectation values are found directly from sequence probabilities, as follows:

$$\begin{aligned} \langle s_i s_{i+1} \rangle &= P(11) + P(00) - 2P(01) \\ &= 1 - 4P(01) \\ \langle s_i s_{i+2} \rangle &= P(111) + P(101) + P(000) + P(010) \\ &\quad - 2P(110) - 2P(100). \end{aligned} \quad (3)$$

The configurational energy in terms of meV per Zn–S pair is shown in Table 4 for several crystalline structures and for each of the four disordered samples. The configurational energies are bounded above and below by the 2H and 3C structures with relative configurational energies of 1.95 meV per Zn–S pair and −1.79 meV per Zn–S pair, respectively. For SK134, the annealing process has introduced faults and has lowered the average configurational energy from the original 2H structure to 1.13 meV per Zn–S pair, while increasing the configurational entropy. If we assume that SK137 is a partially transformed 2H-to-3C crystal [though mostly 3C], then we see that the crystal experiences further disordering and the configurational energy falls to −0.57 meV per Zn–S pair. SK135 shows the most advanced transformation with the 2H structure almost completely eliminated and configurational energy not too far from the ideal minimum at −1.02 meV per Zn–S pair. The configurational entropy begins to fall, however, as the transformation nears a disordered 3C crystal. Being only a slightly disordered 2H crystal, SK229 shows the highest configurational energy of 1.56 meV per Zn–S pair. As we might expect from the relative magnitudes of J_1 and J_2, the contribution from the J_1 term completely dominates the energy.

4.4. Hexagonality

The degree of birefringence of ZnS crystals is known to depend only a single structural parameter – the hexagonality α_h (Brafman & Steinberger, 1966). This parameter is defined as the fraction of MLs which are hexagonally related to their neighbors. That is, α_h is defined as the frequency of occurrence of sequences ABA and BAB and their cyclic permutations. In terms of the Hägg notation, these are simply $P(01)$ and $P(10)$, respectively. Since $P(01) = P(10)$ (Varn *et al.*, 2007*a*), we have

$$\alpha_h = 2P(01). \quad (4)$$

Sequence probabilities are directly calculable from the ε-machine, so that the hexagonality of a disordered crystal can be easily found.

In Table 4 we show the hexagonality calculated for all the spectra, as well as for several crystal structures for comparison. We make several observations. The first is that the hexagonality is strongly correlated with the configurational energy (a high hexagonality implies a high configurational energy). This is to be expected, as the configurational energy term is dominated by the J_1 term, which itself is strongly dependent on the $P(01)$ sequence. The $P(01)$ also determines the hexagonality. We also see that the 6H crystal structure has a higher hexagonality and configurational energy than the one disordered spectrum, SK135. This suggests that during a solid-state transformation initiating in the 2H structure, a disordered 3C, rather than a 6H crystal, is the more likely end result. This is in agreement with experiment for ZnS. Other materials, such as SiC, may follow different routes to disorder due, in part, to different J_i and K_i terms.

5. Discussion

We have successfully applied computational mechanics to the discovery and description of stacking order in single crystals of polytypic ZnS. In doing so, we reconstructed from experimental diffraction spectra the minimal, optimal and unique description of the stacking process as embodied in the ε-machine. In contrast to previous analyses (Sebastian & Krishna, 1994), we used *all* of the information in the diffraction spectra, both in the Bragg peaks and in the diffuse scattering between them. We imposed no restrictions on the kind of structures to be found, save that they be representable by ε-machines. Further, the computational mechanics approach was not limited to the case of weak faulting, but can be used to treat even highly disordered samples. Additionally, the ε-machine can naturally accommodate more than one parent crystalline structure, as seen in SK134.

For two of the spectra, a sensible decomposition[3] of the ε-machine into crystal and faulting structure was possible, allowing a direct comparison between the computational mechanics approach and the FM. The ε-machine detected structures not previously found by the FM. For example, in SK134 we found that not only was structure associated with deformation faulting important, but there was also structure related to growth faults and layer-displacement faulting. We even found nascent sequences leading to the 3C structure. For the other two cases, while no FM-like decomposition of the ε-machine was proposed, we still found significant structure as embodied in the ε-machine. From the ε-machine, physical insight into the structure of the stacking was possible. For example, in the $r = 3$ reconstructed ε-machine for SK137 we could eliminate 6H structure based on the absence of a transition between CSs. We also found that 2H structure was present. Even when no sensible decomposition into a simple

[3] Recall that this decomposition is not unique because of the assumptions used in the FM (Varn *et al.*, 2007*a*).

pure-crystal and weak-faulting structure is possible, the ε-machine still directly provides sequence frequencies, which can be used to build physical insight into the stacking structure.

From a knowledge of the ε-machine, it is possible to calculate a number of physical characteristics. In Table 3 we tabulated the configurational entropy per ML for each sample. Given the coupling parameters between MLs we calculated the average configurational energy for the samples, as shown in Table 4. We were also able to find the hexagonality for the disordered crystals. Knowing the ε-machine allowed us to find various characteristic lengths associated with each disordered crystal, such as the memory length and the generalized period. We believe that additional physics can be calculated from the ε-machine.

We also calculated measures of intrinsic computation from the ε-machine. We found that the minimum memory length for all samples was $r = 3$, which is in excess of the calculated inter-ML interaction range of ~ 1 ML for ZnS. We further found that the statistical complexity, a measure of the amount of information stored by the stacking process, was also much larger than that of either the pure 2H or 3C structures. Also, the range over which structures are found in the disordered samples is ~ 6 ML.

Characterizing solid-state transitions in polytypic materials is of considerable interest. Let us review what an ε-machine does and does not imply. Most simply put, the ε-machine is the answer to the question, 'What is the minimal, optimal and unique description of the one-dimensional stacking structure of the sample?' Any physical parameters that depend on this description are *in principle* calculable from the ε-machine. The ε-machine does *not* answer the question, 'How did the crystal come to be stacked in this way?' To determine this, one must augment the structural knowledge (as embodied in the ε-machine) with additional information or assumptions. Such information can come in the form of a time series of structures obtained either from a series of numerical simulations or experiments or, in the theoretical domain, perhaps from assumptions about weak faulting.

Since we have discovered structures in polytypic ZnS that were undetected before, we feel that the mechanism of faulting – previously attributed to deformation faulting – deserves re-examination. We have provided a firm theoretical foundation for the discovery and description of disordered stacking sequences in polytypes and believe that additional experimental studies are warranted. Additionally, computer simulations of solid-state transformations in polytypes with proposed faulting mechanisms, accompanied by the concomitant reconstruction of the ε-machine directly from the sequence of MLs from the simulation, should provide a powerful method to understand the gross features of the transformations (Varn & Crutchfield, 2004).

Before such studies can be definitive, a quantitative understanding of the effects of experimental error on the reconstructed ε-machine is needed. With the exception of our introduction of the figures-of-merit, γ and β, we have not addressed this important issue here. We note that the original experimental data were not reported with error bars and this means that comparison with the desired ε-machine error analysis would not have been possible. Additionally, the necessity to digitize the data undoubtedly introduced errors. It is therefore difficult to assess the amount of error in each spectrum. Our intuition tells us that error in the diffraction spectrum will likely lead to suppression of the more delicate structures on an ε-machine. Therefore, one should expect to find *less* structure and *more* randomness.

We mention that the application of computational mechanics to the description of one-dimensional sequences is the most general approach possible to this problem. Thus, its application here to polytypism represents the end point in the evolution of models to describe the disordered sequences seen in these substances. Any alternate description can be expressed as an equivalent ε-machine and none can be more general, since in the language of statistics an ε-machine is the minimal sufficient statistic for the underlying process. It may be possible to find specialized algorithms that are more sensitive or more efficient in determining an ε-machine than the one we introduced in εMSR. However, the answer, in its most general form, will be expressible as an ε-machine.

We also note that our work here represents a solution to a significant theoretical problem: how does one extract structural information from a power spectrum? Our application has been to polytypism, but the principles underlying our solution may be applied quite generally to domains in which spectral information is available.

Future directions for this work include an application of εMSR to other polytypes, as well as to substantially more complex materials. The extension of these ideas to the more common cases of disorder in two and three dimensions is also desirable. The development of computational mechanics in higher dimensions would significantly aid in the classification and understanding of disorder in many physical systems. Some recent progress has been made on the understanding of the pattern and computation in higher dimensions (Lindgren *et al.*, 1998; Feldman, 1998; Feldman & Crutchfield, 2003; Young *et al.*, 2005).

We thank D. P. Feldman, R. Haslinger, C. Moore, C. R. Shalizi and E. Smith for helpful conversations. This work was supported at the Santa Fe Institute under the Networks Dynamics Program funded by the Intel Corporation and under the Computation, Dynamics, and Inference Program *via* SFI's core grants from the National Science and MacArthur Foundations. Direct support was provided by NSF grants DMR-9820816 and PHY-9910217 and DARPA Agreement F30602-00–2-0583. DPV's original visit to SFI was supported by the NSF.

References

Akizuki, M. (1981). *Am. Mineral.* **66**, 1006.
Brafman, O. & Steinberger, (1966). *Phys. Rev.* **143**, 501–505.
Brindley, G. W. (1980). *Crystal Structures of Clay Minerals and their X-ray Identification*, edited by G. W. Brindley & G. Brown, ch. II. London: Mineralogical Society.

Crutchfield, J. P. & Young, K. (1989). *Phys. Rev. Lett.* **63**, 105–108.
Engel, G. E. (1990). *J. Phys. Condens. Matter*, **2**, 6905–6919.
Feldman, D. P. (1998). PhD thesis. University of California, Davis.
Feldman, D. P. & Crutchfield, J. P. (1998). Santa Fe Institute Working Paper 98–04-026.
Feldman, D. P. & Crutchfield, J. P. (2003). *Phys. Rev. E*, **67**, 051104.
Frank, F. C. (1951). *Philos. Mag.* **42**, 1014.
Frey, F., Jagodzinski, H. & Steger, G. (1986). *Bull. Mineral.* **109**, 117–129.
Frondel, C. & Palache, C. (1948). *Science*, **107**, 602.
Frondel, C. & Palache, C. (1950). *Am. Mineral.* **35**, 29–42.
Gosk, J. B. (2000). *Crys. Res. Tech.* **35**, 101–116.
Gosk, J. B. (2001). *Cryst. Res. Technol.* **36**, 197–213.
Hahn, T., Wilson, A. J. C. & Shmueli, U. (1992). Editors. *International Tables for Crystallography*, 3rd ed. Dordrecht: Kluwer Academic Publishers.
Jagodzinski, H. (1949*a*). *Acta Cryst.* **2**, 201–207.
Jagodzinski, H. (1949*b*). *Acta Cryst.* **2**, 208–214.
Jagodzinski, H. (1949*c*). *Acta Cryst.* **2**, 298–304.
Jagodzinski, H. (1954). *Acta Cryst.* **7**, 300.
Kabra, V. K. & Pandey, D. (1988). *Phys. Rev. Lett.* **61**, 1493–1496.
Keen, D. A. & McGreevy, R. L. (1990). *Nature*, **344**, 423–425.
Lindgren, K., Moore, C. & Nordahl, M. (1998). *J. Stat. Phys.* **91**, 909–951.
Mardix, S. (1986). *Phys. Rev. B*, **33**, 8677–8684.
Michalski, E. (1988). *Acta Cryst.* A**44**, 640–649.
Milburn, G. H. W. (1973). *X-ray Crystallography: An Introduction to the Theory and Practice of Single-Crystal Structure Analysis.* Butterworth and Company.
Müller, H. (1952). *Neues Jahrb. Mineral. Abh.* **84**, 43–76.
Pandey, D., Prasad, L., Lele, S. & Gauthier, J. P. (1987). *J. Appl. Cryst.* **20**, 84–89.
Price, G. & Yeomens, J. (1984). *Acta Cryst.* B**40**, 448.
Proffen, T. & Welberry, T. R. (1998). *Phase Transit.* **67**, 373–397.
Roth, W. L. (1960). *Faulting in ZnS.* Technical Report 60-RL-2563M. General Electric Research, Schenectady, New York.
Sebastian, M. T. (1988). *J. Mater. Sci.* **23**, 2014–2020.
Sebastian, M. T. (2001). Private communication.
Sebastian, M. T. & Krishna, P. (1984). *Philos. Mag. A*, **49**, 809–821.
Sebastian, M. T. & Krishna, P. (1987*a*). *Cryst. Res. Tech.* **22**, 929–941.
Sebastian, M. T. & Krishna, P. (1987*b*). *Cryst. Res. Tech.* **22**, 1063–1072.
Sebastian, M. T. & Krishna, P. (1994). *Random, Non-Random and Periodic Faulting in Crystals.* Gordon and Breach.
Sebastian, M. T., Pandey, D. & Krishna, P. (1982). *Phys. Status Solidus A*, **71**, 633–640.
Shalizi, C. R. & Crutchfield, J. P. (2001). *J. Stat. Phys.* **104**, 817–881.
Shaw, J. J. A. & Heine, V. (1990). *J. Phys. Condens. Matter*, **2**, 4351–4361.
Shrestha, S. P. & Pandey, D. (1996*a*). *Europhys. Lett.* **34**, 269–274.
Shrestha, S. P. & Pandey, D. (1996*b*). *Acta Mater.* **44**, 4949–4960.
Shrestha, S. P. & Pandey, D. (1997). *Proc. R. Soc. London Ser. A*, **453**, 1311–1330.
Shrestha, S. P., Tripathi, V., Kabra, V. K. & Pandey, D. (1996). *Acta Mater.* **44**, 4937–4947.
Singer, J. & Gashurov, G. (1963). *Acta Cryst.* **16**, 601–604.
Steinberger, I. I. (1983). *Crystal Growth and Characterization of Polytype Structure*, edited by P. Krishna. Oxford: Pergamon Press.
Thompson, J. B. (1981). *Structure and Bonding in Crystals* II, edited by M.O'Keefe & A. Navrotsky, ch. 22. New York: Academic Press.
Trigunayat, G. C. (1991). *Solid State Ion.* **48**, 3–70.
Varn, D. P. (2001). PhD thesis, University of Tennessee, Knoxville.
Varn, D. P. & Canright, G. S. (2001). *Acta Cryst.* A**57**, 4–19.
Varn, D. P., Canright, G. S. & Crutchfield, J. P. (2002). *Phys. Rev. B*, **66**, 174110.
Varn, D. P., Canright, G. S. & Crutchfield, J. P. (2007*a*). Submitted for publication
Varn, D. P., Canright, G. S. & Crutchfield, J. P. (2007*b*). Submitted for publication.
Varn, D. P. & Crutchfield, J. P. (2004). *Phys. Lett. A*, **324**, 299–307.
Varn, D. P. & Crutchfield, J. P. (2006). Unpublished.
Verma, A. R. & Krisha, P. (1966). *Polymorphism and Polytypism in Crystals.* New York: John Wiley and Sons.
Warren, B. E. (1969). *X-ray Diffraction.* Boston, MA: Addison–Wesley.
Welberry, T. R. & Proffen, T. (1998). *J. Appl. Cryst.* **31**, 309–317.
Woolfson, M. M. (1997). *An Introduction to X-ray Crystallography.* Cambridge University Press.
Yeomans, J. (1988). *Solid State Phys.* **41**, 151–200.
Young, K., Chen, Y., Kornak, J., Matson, G. B. & Schuff, N. (2005). *Phys. Rev. Lett.* **94**, 098701.